Oil & Gas Science and Technology — Rev. IFP Energies nouvelles

DOI: will be set by the publisher

Numerical methods and turbulence modeling for LES of piston engines: impact on flow motion and combustion

A.Misdariis[1,2], A.Robert[3,4], O.Vermorel[2], S.Richard[3] and T.Poinsot[2]*

1 Renault SAS, 1 Av. du Golf, 78288 Guyancourt Cedex, France
2 CERFACS, 42 Av. G. Coriolis, 31057 Toulouse Cedex 01, France
3 IFP Energies nouvelles, 1-4 avenue de Bois Préau, 92852 Rueil-Malmaison
4 PSA, Route De Gisy, 78943 Velizy Villacoublay, France

e-mail: antony.misdariis@cerfacs.fr — anthony.robert@ifpen.fr

*Corresponding author

Résumé — Cet article présente une évaluation de l'impact du set-up numérique sur les processus d'écoulement et de combustion prédits par Simulation aux Grandes Echelles (SGE) dans les moteurs à combustion interne. Du fait de la complexité et du coût important de calcul associés à ce type de simulation, le set-up le plus classique consiste à utiliser des schémas d'ordre faible (typiquement premier ou second ordre en temps et en espace) et des modèles de turbulence de sous-maille simples (comme le modèle de Smagorinsky [30]). L'objectif de ce travail est donc d'évaluer la faisabilité de l'utilisation de méthodes plus précises, combinant schémas d'ordre élevé et modèles de sous-maille avancés, ainsi que les bénéfices potentiels associés. Pour cela, deux schémas de convection de la famille Two-step Taylor Galerkin (TTG) [5] ainsi que différents modèles de turbulence, à savoir Smagorinsky dynamique [12] et sigma [31], sont retenus et comparés au set-up conventionnel Lax-Wendroff (LW) [22] - Smagorinsky. Pour mener à bien cette étude, deux configurations de moteurs à allumage commandé de l'IFPEN dédiées spécifiquement à la validation de la SGE sont simulées. La première est le moteur atmosphérique F7P, à quatre soupapes par cylindre qui dispose d'une caractérisation exhaustive, à la fois expérimentale et numérique. La seconde est le moteur Ecosural, qui est équipé d'une injection directe et est fortement suralimenté. Une unique réalisation de cycle moteur est simulée pour chacun des set-up et la comparaison s'appuie sur les résultats expérimentaux et numériques du moteur F7P qui a l'avantage de bénéficier des enveloppes de variabilité cyclique. Les résultats expérimentaux du moteur Ecosural n'étant pas encore disponibles, les comparaisons réalisées restent qualitatives, mais ont l'intérêt de confirmer ou d'infirmer les observations établies sur le F7P dans des conditions de fonctionnement très différentes. Concernant les modèles de sous maille, seules de faibles différences sont trouvées au niveau aérodynamique, même si le modèle sigma permet une meilleure résolution des petites structures du champ de vitesse. Les évolutions des différentes grandeurs se maintiennent en effet dans les enveloppes de variabilité cycle à cycle de Granet et al. [16] sans claire amélioration sur les grandeurs macroscopiques telles que l'énergie cinétique résolue, le dégagement de chaleur ou la pression cylindre moyenne. Les tests des différents schémas numériques montrent que ceux de la famille TTG permettent également une description légèrement mieux résolue du champ de vitesse,

mais les grandeurs globales telles que l'énergie cinétique résolue ou la viscosité turbulente moyenne restent à des niveaux comparables à ceux de LW. Néanmoins, des écarts importants de comportement apparaissent pendant la phase de combustion. Ces écarts sont attribués à une meilleure résolution du processus d'interaction flamme/turbulence pendant la phase de propagation libre, ce qui se traduit par un niveau de dégagement de chaleur résolu sur le maillage accru. Une étude montre également que la constante du modèle de dégagement de chaleur de sous-maille du modèle de flamme épaissi doit être modifiée lorsque les schémas TTG sont utilisés afin de prendre en compte l'augmentation de la partie résolue du dégagement de chaleur. L'ensemble des ces travaux conduisent à la proposition d'une approche hybride appelée ESO_2 qui consiste à utiliser les schémas TTG pendant la combustion et le schéma LW pour les autres phases du cycle. Cette approche est testée sur les deux configurations moteur et permet d'obtenir des résultats comparables à ceux du schéma TTGC seul pour un coût de calcul fortement réduit. La précision du schéma LW semble donc suffisante pour les phases d'admission et de compression tandis que l'utilisation du schéma TTGC pendant la combustion permet une augmentation de la qualité des SGE. Finalement la méthode ESO_2 apparaît comme une approche attractive pour améliorer la précision des simulations sans être pénalisé par des coûts de calcul prohibitifs dans les simulations multi-cycles.

Abstract *— In this article Large Eddy Simulations (LES) of Spark Ignition (SI) engines are performed to evaluate the impact of the numerical set-up on the predicted flow motion and combustion process. Due to the high complexity and computational cost of such simulations, the classical set-up commonly includes "low" order numerical schemes (typically first or second-order accurate in time and space) as well as simple turbulence models (such as the well known constant coefficient Smagorinsky model [30]). The scope of this paper is to evaluate the feasibility and the potential benefits of using high precision methods for engine simulations, relying on higher order numerical methods and state-of-the-art sub-grid-scale (SGS) models. For this purpose, two high order convection schemes from the Two-step Taylor Galerkin (TTG) family [5] and several SGS turbulence models, namely Dynamic Smagorinsky [12] and sigma [31] are considered to improve the accuracy of the classically used Lax-Wendroff (LW) [22] Smagorinsky set-up. This evaluation is performed considering two different engine configurations from IFPEN. The first one is the naturally aspirated four valve spark-ignited F7P engine which benefits from an exhaustive experimental and numerical characterization. The second one, called Ecosural, is a highly supercharged spark-ignited engine. Unique realizations of engine cycles have been simulated for each set-up starting from the same intial conditions and the comparison is made with experimental and previous numerical results for the F7P configuration. For the Ecosural, experimental results are not available yet and only qualitative comparisons are performed to enforce the analysis and conclusions made on the F7P. Regarding SGS models, only slight differences are found at the aerodynamic level even if sigma allows a better resolution of small structures of the velocity field. However, all results are in cycle-to-cycle variability envelopes from Granet et al. [16] and these single cycle computations don't permit to distinguish clear improvements on macroscopic parameters such as resolved kinetic energy, heat release or mean in-cylinder pressure. Concerning numerical schemes, TTG schemes also allow a slighlty better resolution of small scale vortices but global quantities such as resolved kinetic energy and SGS viscosity are comparable. Nevertheless, clear differences appear between the different schemes in the combustion stroke. This is attributed to a better resolution of the flame-turbulence interaction process during the free flame propagation period, leading to an increase of the resolved part of heat release. It is also shown in this paper that an adjustment of the efficiency constant in the Thickened Flame (TF) model is compulsory to account for this better resolution if TTG schemes are used. In the light of these conclusions an hybrid set-up, called* ESO_2*, which consists in using TTGC during combustion and LW elsewhere is proposed and applied to the two engines configurations. Results are in good agreement with the ones obtained in the case of a full TTGC simulation, while the CPU cost increase is only about* 10% *compared to LW. The accuracy of LW seems therefore to be sufficient for pure aerodynamic phases, while the use of TTGC only during combustion permits an improvement in the LES quality. The hybrid* ESO_2 *method thus appears as an attractive approach to improve further calculations accuracy without being greatly penalized by additional CPU costs in multi-cycle simulations.*

1 INTRODUCTION

In the past few years, Large Eddy Simulation (LES) has been a subject of growing interest from the automotive community because of its unique potential to reproduce unsteady and sporadic phenomena like cycle-to-cycle variations (CCV) or abnormal combustions [3, 11, 13, 17, 28, 32]. However, Internal Combustion Engines (ICE) still remain a recent and complex field of application for LES: the flow is highly unsteady and governed by a strong interaction between numerous physical phenomena (turbulence, mixing, combustion, multi-phase flows, acoustics,...), the geometry is mobile and initial and boundary conditions are generally badly characterized or defined (wall temperature, inlet/outlet pressure or velocity signal). When dealing with sporadic or erratic phenomena such as CCV or abnormal combustions, an additional difficulty arises: since reliable trends and statistics may only be obtained by computing numerous cycles (typically 50), the solver must necessarily be robust and fast. A direct consequence of these issues (complexity, novelty, cost and robustness) is that classical ICE simulations do not generally use "high order" set-up compared to more academic LES configurations, such as turbulent pipe flows for instance [24], for which highly accurate set-up are the standard. In particular, ICE simulations usually use low order and/or dissipative numerical schemes as well as simple sub-grid scale (SGS) turbulence models. Concerning numerical schemes, two classes of convective schemes are generally found in the literature: upwind-biased schemes are used by Jhavar and Rutland [18], Dugue *et al.* [7] or Goryntsev *et al.* [13] for instance while low order centered schemes (second order accurate in space and time at most) are used by Richard *et al.* [28], Vermorel *et al.* [32] or Granet *et al.* [16]. Both of them are known to be very dissipative and a priori not well suited for LES. Concerning turbulence modeling, the most popular closure is the constant coefficient Smagorinsky model [30]. In spite of its well-known drawbacks [12], this model is used in many ICE LES, such as Goryntsev *et al.* [13], Celik *et al.* [2], Vermorel *et al.* [32] or Granet *et al.* [16]. The combined use of a low order numerical scheme and a simple turbulence model does not mean that the results of these computations are systematically wrong or dubious. Many other parameters have also to be taken into account (the resolution and the quality of the grid especially) to state if a methodology is adequate or not. Besides, many promising results have been obtained with such a set-up. For example, previous works conducted at IFPEN and CERFACS using the Lax-Wendroff scheme (second order in time and space) and the classical constant coefficient Smagorinsky model have demonstrated the great potential of LES for solving complex problems in piston engines, notably its ability to help understanding CCV sources [8, 16, 32] and to build phenomenological models for engine control development [25].

However, it is well known that both numerics and turbulence models can have a huge impact on the simulation results. In the perspective of using LES for predicting engine operation far upstream in its design process, highly precise methods should then be used to provide more reliable results. This objective is laudable but not necessarily realistic: high order non-dissipative schemes generally exhibits high-frequency artificial oscillations, which may cause instability in the computations and jeopardize the robustness of the solver. High order set-up may also lead to prohibitive computational costs for engine simulations, which require tens of cycles for generating reliable converged statistics. The objective of this work is therefore to evaluate the feasibility and the potential benefits (or drawbacks) of using high precision numerical schemes and state-of-the-art SGS turbulence models in terms of precision, robustness and cost. For this purpose, two convective schemes from the Two-step Taylor-Galerkin (TTG) family are tested and evaluated in combination with several SGS models (Smagorinsky, dynamic Smagorisnky, sigma). This evaluation is performed considering two different engine configurations of IFPEN : a naturally aspirated engine and a highly supercharged engine. Thanks to these comparisons, an optimal set-up is highlighted and a new approach called ESO_2 (Engine Stroke Optimal Order) method, based on the choice of the best compromise in terms of CPU cost and precision, is proposed.

2 TEST CASE DESCRIPTION AND APPROACH

The aim of the present study is to propose an appropriate numerical set-up which would be able to handle piston engine simulations with the highest fidelity. For this purpose, three different numerical schemes and three different SGS models are evaluated and compared on two different engine configurations. The three numerical schemes are the classical finite volume Lax-Wendroff (LW) scheme [22] (2^{nd} order accurate in space and time) and two finite element (FE) schemes from the 2-step Taylor-Galerkin family: TTGC (3^{rd} order accurate in space and time) and TTG4A (4^{th} order accurate in time and 3^{rd} order accurate in space) [5]. For academic configurations (convection of a vortex, HIT), these two FE schemes give much better results than the LW scheme thanks to their better dispersive and dissipative properties [5]. They have also been widely and successfully used in complex configurations such as gas turbine combustion chambers in recent LES studies [10, 27, 29, 33]. Concerning the SGS models, in addition to the classical constant coefficient Smagorinsky model [30], two more recent closures are also evaluated: the dynamic Smagorinsky [12] and the

sigma [31] models. Many studies have already highlighted the conceptual and actual advantages of the dynamic procedure compared to the constant coefficient method [23, 26]. The sigma model is also supposed to give better results than the classical Smagorinsky model, especially in the vicinity of solid boundaries or in case of pure shear and solid rotation for instance [31]. The two configurations are the F7P and the Ecosural single cylinder engines from IFPEN. The F7P configuration has been widely studied experimentally and numerically in previous works. In [8, 9, 16], multi-cycle LES of different motored and reactive operating points are presented. The numerical set-up includes a LW convection scheme and a constant coefficient Smagorinsky model. Despite its supposed "low" accuracy, this set-up exhibited promising results: for various operating points, experimental results in terms of aerodynamics and combustion cycle-to-cycle variability were correctly reproduced not only qualitatively but also quantitatively. The Ecosural engine is a modern single cylinder engine, specifically designed to support research activities on very efficient engines. Experimental measurements are currently performed at IFPEN on the Ecosural to provide LES dedicated data, but were not available for this study. For this reason, only qualitative comparisons between the different numerical set-up are achieved, with the aim to support or infer conclusions drawn on the F7P engine. Such results are nevertheless particularly interesting since the engine design and operating conditions (engine load, speed) are very different from those of the F7P.

2.1 Methodology

Since SI engines configurations can exhibit important levels of cycle-to-cycle variations, the best way to evaluate the above cited numerical schemes and turbulence models would be to perform multi-cycle computations and to compare statistical results over several tens of cycles. Unfortunately, the computational cost associated to the simulation of these numerous cycles prevents the use of this strategy for all the numerical tests. Thereby it has been chosen to perform a unique cycle calculation for each numerical scheme and turbulence model. Each computation starts at intake valve opening (IVO) from the same initial conditions and ends after the combustion process. The comparison between the different set-up is performed at three levels of interest: trapped mass, flow field and combustion process. It is worth noting that this single-cycle strategy introduces a severe difficulty when comparing the results: it may be difficult to separate the differences due to a change in the numerical set-up from the differences due to "natural" cycle-to-cycle variations. In that sense, the objective here is not to establish a definitive hierarchy between the different numerical schemes and SGS models, but only to bring new elements for future computations and to point out some possible unphysical behaviors as well.

2.2 Engine configurations

The first single cylinder configuration is the F7P engine [20, 21]. It is fully equipped with sensors and optical accesses and benefits from a full experimental and numerical characterization on several operating points and a extensive database is then available for comparison. This naturally aspirated configuration consists in a single-cylinder four-valve spark-ignition engine fueled with gaseous propane (Figure 1). Its main specifications are given in Table 1.

TABLE 1
Main engine specifications. Crank Angle Degrees (CAD) are relative to compression Top-Dead-Center (TDC).

	Unity	
Geometrical compression ratio	-	9.9
Engine speed	rpm	1200
Bore	mm	82
Stroke	mm	83,5
Connecting rod length	mm	144
Intake valve opening/closing	CAD	350/-120
Exhaust valve opening/closing	CAD	120/-350
LES grid (million tetrahedra)	-	2.2 to 9.6

The operating point chosen for this study is the one named *unst_dil* in Granet *et al.* [16]. This condition is called "unstable" because of its high degree of CCV (COV_{IMEP} = 7.2%, see Table 2). Compared to a stable operating point, it is expected to exhibit differences between the different set-up.

TABLE 2
Experimental characteristics of *unst_dil* operating point.

	Unity	
Fuel	-	C3H8
Equivalence ratio	-	1
Dilution by N2	% vol.	0.32
Trapped mass	mg	250
Spark advance	CAD	50
Mean IMEP	bars	3.19
COV (IMEP)	%	7.2
Mean Pmax	bars	16.9
COV (Pmax)	%	12.4

As mentioned in section 2.1, the comparison of the different set-up are only based on single-cycle computations due to their high computational cost, which may complicate the analysis and the conclusions. In order to enforce (or not) these conclusions, a second test configuration is also studied. This second configuration is a highly downsized spark ignition engine (Fig. 2) recently developed at IFPEN for the ICAMDAC project [1]. It is equipped with direct injection and is characterized by a high tumble ratio aiming

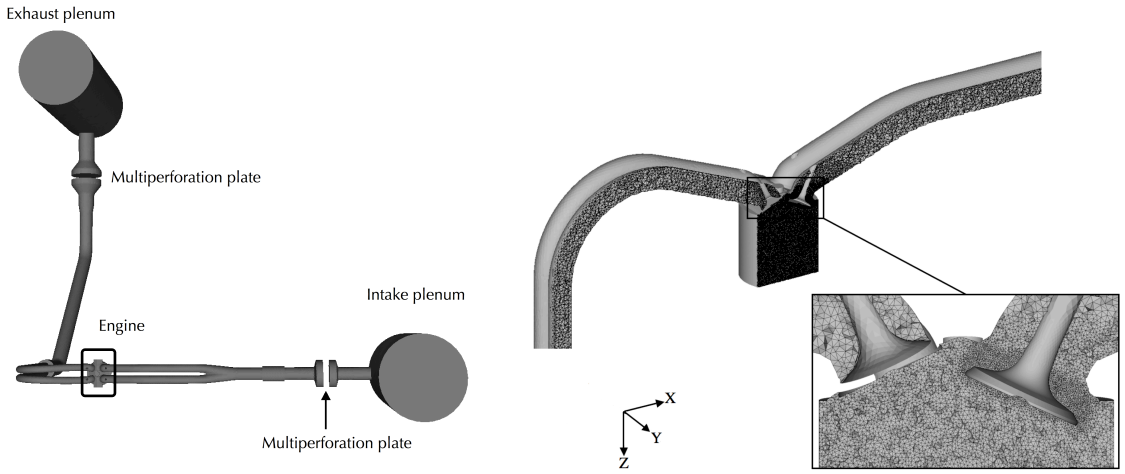

Figure 1
Sketch of the experimental F7P engine test bench (left) and view of a typical tetrahedral mesh during the intake stroke [9](right).

at generating important levels of turbulence in the combustion chamber. It can therefore support elevated boost levels and IMEP (indicated mean effective pressure) of the order of 30 bars. Table 3 summarizes the main specifications of the Ecosural engine. In order to bring complementary elements compared to the F7P case, very different operating conditions are voluntary chosen, namely both engine speed and load are increased (Table 4) to mimic a near knocking condition called *knock* in the following. In practice, gasoline and iso-octane will be experimentally tested in this engine, but gaseous propane is used for this qualitative study in order to avoid fuel stratification effects and to facilitate comparisons with the F7P simulations.

TABLE 3
Main engine specifications. CAD are relative to compression TDC.

	Unity	
Geometrical compression ratio	-	10.5
Engine speed	rpm	1800
Bore	mm	77
Stroke	mm	85.8
Connecting rod length	mm	132.2
Intake valve opening/closing	CAD	353/-156
Exhaust valve opening/closing	CAD	116.5/-353.5
LES grid (million tetrahedra)	-	2.2 to 12.2

2.3 Numerical set-up

All the computations are performed with the AVBP LES code [14, 15], which solves the compressible multi-species Navier-Stokes equations. The Energy deposition [19] and TFLES models [6] are respectively used to simulate spark ignition and flame propagation, as in [16]. Simulation grids are made of tetrahedra, allowing to refine small scale turbulence zones around the valves during intake or in the spark plug vicinity at spark timing, while using coarsened meshes at the intake and exhaust (Fig. 1 and 2). Due to the piston movement, the number of cells highly evolves during the computation and ranges from about 2 millions at top dead center (TDC) to around 10 millions at bottom dead center (BDC) depending on the engine (Table 1 and 3). Computational ressources necessary to simulate one cycle are about 30 hours on 400 processors for each configuration when using the Lax-Wendroff scheme and the Smagorinsky model.

TABLE 4
Experimental characteristics of *knock* operating point.

	Unity	
Fuel	-	C3H8
Equivalence ratio	-	1
Dilution by N2	% vol.	0.0
Trapped mass	mg	844
Spark advance	CAD	20
Mean IMEP	bars	20

3 EVALUATION OF SUB GRID SCALE MODELS

In this section, the constant coefficient Smagorinsky model [30] ($Cs = 0.18$) is compared to its dynamic version [12] and to the sigma closure [31] for both F7P and Ecosural configurations. For all computations, the LW scheme is used and all other parameters (grid, combustion model, CFL, ...) are unchanged. Results are compared to the experimental data and to the reference numerical results (LW-

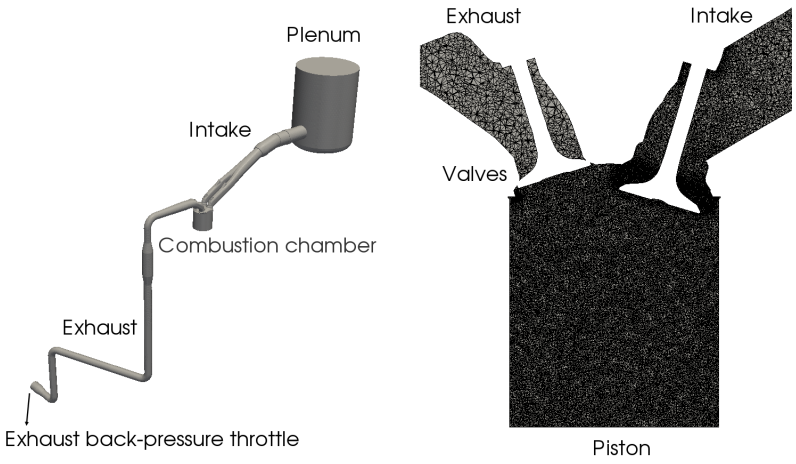

Figure 2

Sketch of the experimental Ecosural engine test bench (left) and view of a typical tetrahedral mesh during the intake stroke (right).

Smagorinsky) reported in [16] for the F7P engine. A qualitative study of the Ecosural simulations is also used to bring complementary element to the F7P LES analysis. In order to identify possible improvements in the results accuracy with these new SGS models, comparisons are first made on trapped mass, then on the flow properties during intake and compression and finally on the combustion process.

3.1 In-cylinder trapped mass

The first macroscopic quantity a piston engine computation should be able to predict is the mass trapped in the cylinder after intake valve closure (IVC) because it has a first order impact on the engine thermodynamic cycle. Most of the time the first cycle of a multi-cycle LES does not allow to get this quantity with precision due to the influence of initial conditions. The present F7P simulations get round the problem by starting from the end of cycle 21 of the *unst_dil* database [16], i.e. from fully realistic initial conditions. For the Ecosural engine, two cycles without combustion are computed using the LW scheme and Smagorinsky model to generate initial conditions for the combustion simulations. As shown in Table 5, for both engine configurations, the differences in trapped mass between the three SGS models are very slight, which means that the influence of the turbulence models on this very macroscopic quantity is almost negligible.

3.2 Intake and compression in-cylinder flow

During the intake and compression strokes, high aerodynamic cycle-to-cycle variations where observed by Enaux

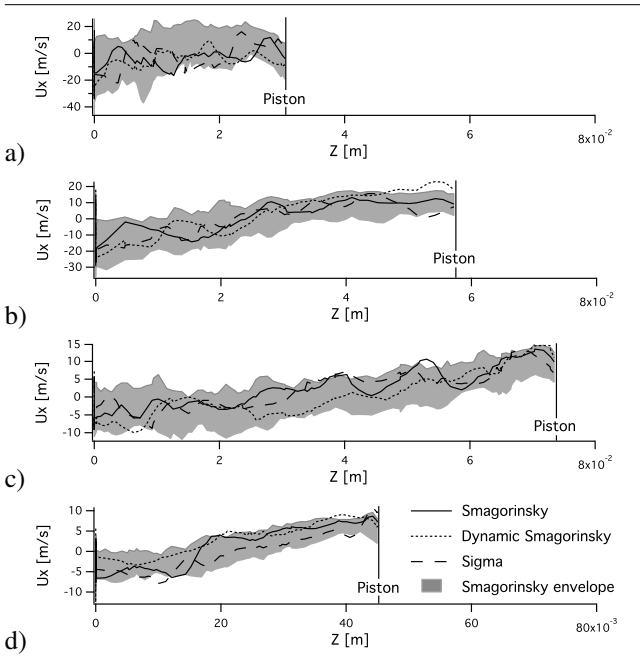

Figure 3

x-velocity profiles along the F7P cylinder axis for the constant Smagorinsky, dynamic Smagorinsky and sigma SGS models at -280 CAD (a), -240 CAD (b), -180 CAD (c) and -100 CAD (d). The constant Smagorinsky envelope is extracted from [16]. The abscissa $z = 0$ corresponds to the bottom of the cylinder head.

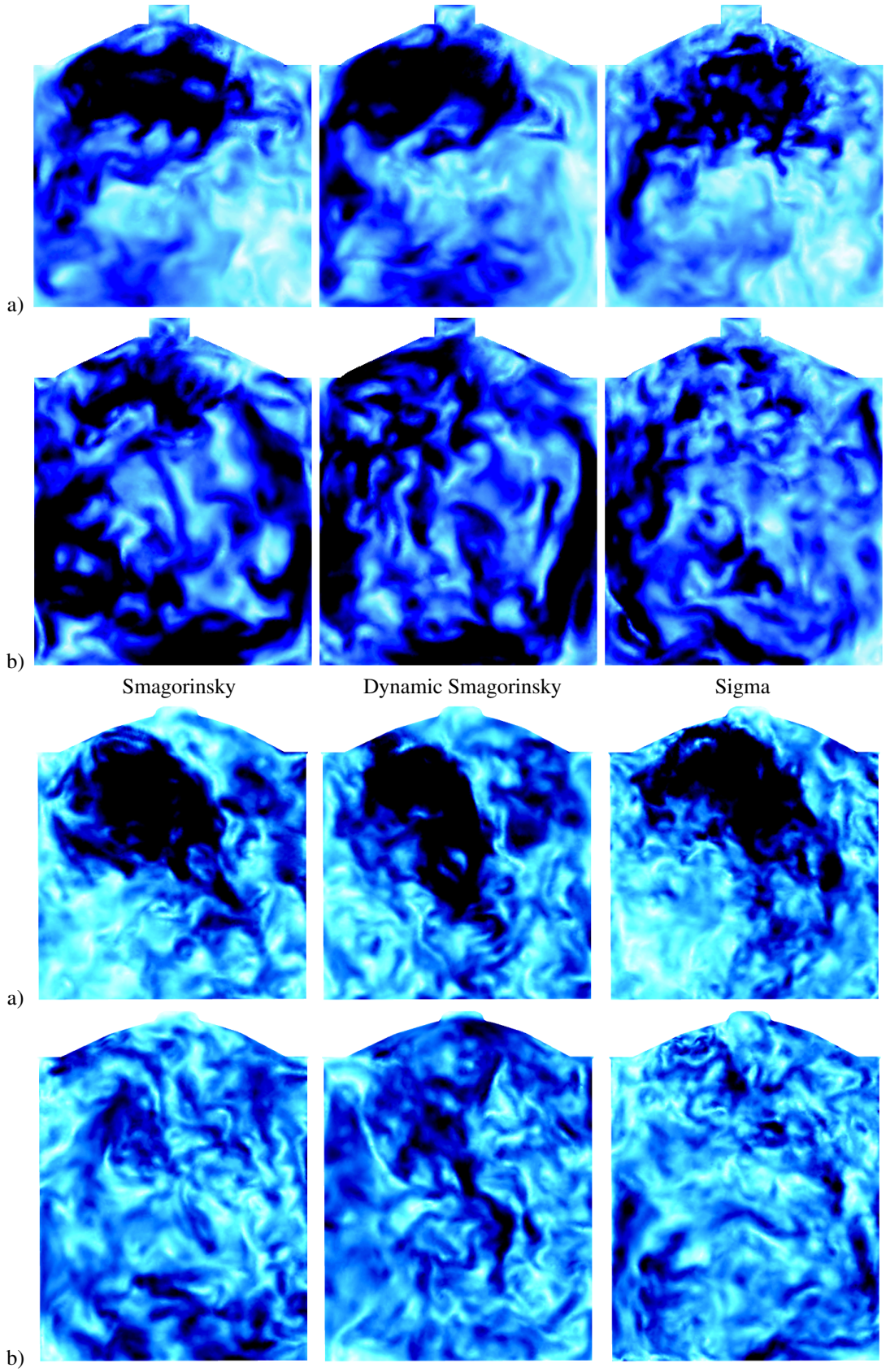

Figure 4

Velocity fields at the F7P (top) and Ecosural (bottom) cylinder center for the constant Smagorinsky, dynamic Smagorinsky and sigma SGS models at different crank angles : -240 CAD (a) and -180 CAD (b).

TABLE 5

Computed trapped mass [mg] for the three SGS models on the two engine configurations.

	Smago.	Dyn. Smago.	sigma
F7P [mg]	254	252	253
Ecosural [mg]	842	843	842

et al. [9] for the motored engine case and Granet *et al.* [16] for the reactive cases of the F7P engine. As an illustration, Fig. 3 shows in grey the statistical envelope of the x-velocity along the cylinder axis $\vec{z}$ for the 50 cycles reported in [16] at four different crank angles (see Fig. 1 for a definition of the axis). Here the statistical envelope of a quantity Q delineates the zone where 95% of the cycles are included and is defined as $Q_{mean}(t) \pm 2\sigma_Q$ with Q_{mean} the mean value of Q and σ_Q its standard deviation. The instantaneous profiles obtained with the constant Smagorinsky, dynamic Smagorinsky and sigma SGS models are also plotted in the same figure. From the aerodynamic point of view, no clear trend appears when comparing the three simulations. All profiles are different, with variations reaching several meters per second, but they remain in the reference envelope. For the two other velocity components (not shown), the same observation can be made. It is all as if every change in the numerical set-up was a simple perturbation introduced in the computation, acting in the same way as a slight modification of the initial conditions for instance.

Although the velocity profiles analysis prevents us to draw conclusions since variations remain in CCV envelopes, plane-cut shown in Fig. 4 (a) permit a further analysis. Large scale motions are very close for the three models and the overall resolved kinetic energy decays presented in Fig. 5 (a) are comparable all along the intake and compression strokes, but a slight difference appears with the sigma closure. This model indeed leads to more distorded velocity fields with smaller structures, indicating that the kinetic energy may not be distributed spatially in the same way as for the other models.

This behavior can be attributed to a lower turbulent viscosity level of the sigma model, as illustred in Fig. 6 (a). This low viscosity was in fact expected since sigma has been built to avoid an over-estimation of the SGS turbulence in shear layers and in solid rotation motion such as tumble in this case [31]. All these statements are confirmed by the Ecosural simulations, which exhibit the same qualitative trends for all physical quantities (Fig. 4, 5 and 6 - (b)) although operating conditions and engine design highly differ from the F7P. Regarding the dynamic Smagorinsky model, it should be noticed that the mean in-cylinder constant, presented in Fig. 7, is very close to the reference value 0.18 of the classical formulation during the intake stroke and progressively differs along the compression, where it increases up to 0.22 for the F7P and 0.25 for the Ecosural due to the effect of the walls. The fact that this increase is lower for

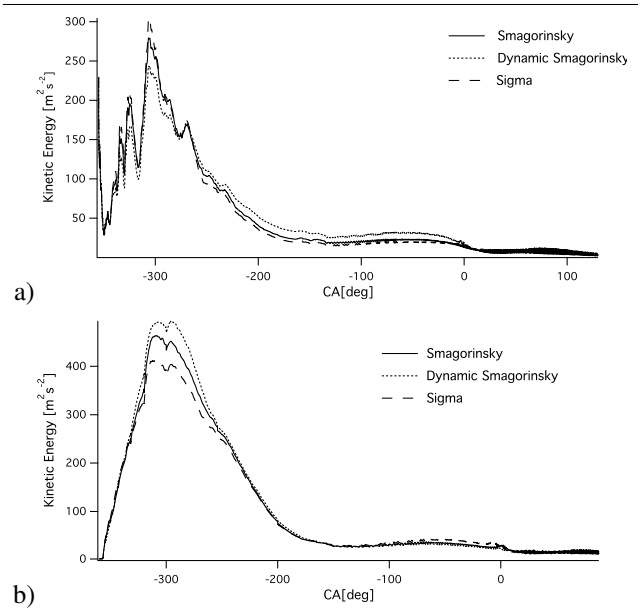

Figure 5

Resolved kinetic energy evolution during the engine cycle for the three SGS models : (a) F7P, (b) Ecosural.

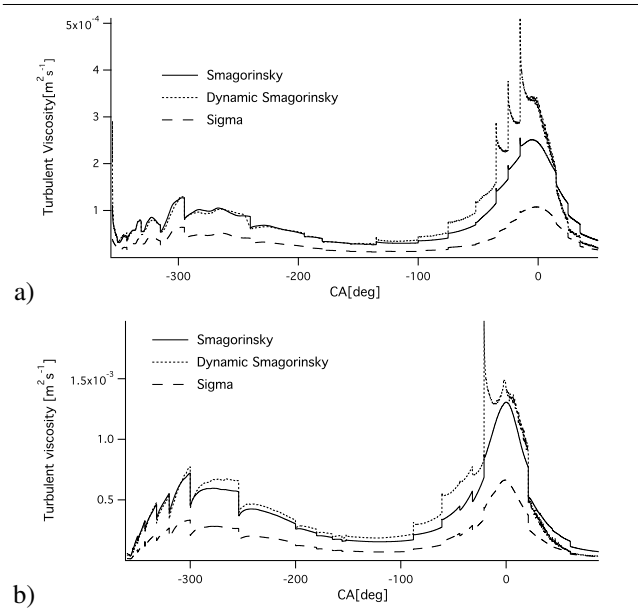

Figure 6

Mean turbulent viscosity in the cylinder for the three SGS models : (a) F7P, (b) Ecosural.

the F7P configuration explains why the two Smagorinsky models present more comparable velocity fields than for the Ecosural engine (Fig. 4). In this last case all the fields have indeed very different shapes. Therefore, it should not be considered as a general conclusion that Smagorinsky and dynamic Smagorinsky simulations result in a comparable

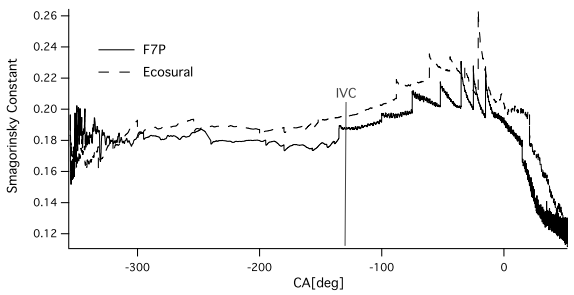

Figure 7

Mean dynamic Smagorinsky model constant in the cylinder for the two engines.

resolved flow before ignition. Another important finding of this study is that even if the SGS viscosity is lower for sigma than for the Smagorinsky models (Fig. 6), the corresponding resolved kinetic energy is not necessarily higher (Fig. 5). This may be because smaller structures induced by the use of sigma are more easily dissipated, while models characterized by a higher SGS viscosity lead to larger scale motions with a greater life-time. In practice both phenomena (small scale and SGS dissipation) will compete and it is difficult to know a priori which one will predomine. A last result concerns the dynamic Smagorinsky model, which exhibits very high levels of SGS viscosity at the walls compared to other closures, as shown in Fig. 8. This observation remains true for both engines and is coherent with the mean in-cylinder constant level at the end of compression. Such a behavior is not physical and may be related to a lack of grid resolution at the walls. Its influence on combustion will be discussed in the following section.

3.3 Combustion stroke

Regarding the combustion process, three phases should be distinguished, as illustrated in Fig. 9. The first one is the free flame propagation period during which the flame kernel generated after spark ignition evolves without being directly constrained by wall effects. During this period, the flame expands rapidly due to the very low density of burned gases compared to the fresh mixture and its wrinkling progressively grows under the action of small scale vortices. The kernel is also convected by large scale motions leading to cyclic variations of its localization. This first phase is crucial since it plays a main role in the combustion event phasing in the cycle. In the second phase of the combustion process, the flame starts interacting with the piston and cylinder head due to the very low height of the combustion chamber around TDC. The reaction zone then propagates towards the periphery of the cylinder while being strongly affected by confinement effects, which vary a lot from one cycle to another. Indeed, the beginning of this phase highly depends on the kernel convection during the free propagation period since the flame can be more or less moved near the walls. The last phase of the heat release is characterized by flame extinction at the cylinder liner due to the decrease of both flame wrinkling and laminar flame velocity. Flame-turbulence interactions are thus not of first order in this part of the engine cycle, which is greatly piloted by heat losses and flow kinetic energy dissipation.
The distinction between these three phases of the combustion stroke is very important because comparisons should be limited to the free flame propagation period. One main reason for this affirmation is that LES analyses are only based on single cycle simulations in this study. Since a modification of the SGS model leads to a slightly different engine cycle realization in terms of flow motion (see previous section), flame kernel convection towards the piston or cylinder head is also affected and the walls influence may highly perturb the models comparison during the second phase. In order to separate effects linked to flame-wall interactions from those directly related to the flow resolution quality itself, a focus is therefore performed on the first combustion phase. During this period, flame propagation processes should be more directly related to the flow charactersitics and thus to the SGS models properties.

The free flame propagation phase lasts around 40 CAD for the F7P and 20 CAD for the Ecosural for all the simulated cycles, as shown in Fig. 10. The flame surface (and thus the heat release) from sigma is higher than those from the Smagorinsky models by a factor around 2 for the two engines. This statement remains true at both resolved and SGS levels, even if the resolved surface highly predomine, especially during flame kernel growth where the SGS heat release represents less than 30% of the total one. This behavior may first be related to the velocity field resolution, which presents more and smaller turbulent structures for sigma. This closure also permits to reduce diffusive fluxes within the reaction zone, allowing potentially to better resolve flame-turbulence interactions even if the velocity field is the same. This last statement was however not verified in this study. Analysing further the flame surface evolution of the F7P, it is interesting to notice that the dynamic Smagorinsky rapidly leads to resolved and SGS quantities close to those of sigma as soon as the flame starts interacting with the walls. This may be linked to the high (and unphysical) values of SGS viscosity in these regions, implying a rapid increase of the SGS wrinkling through the efficiency function of the TFLES model. This tendency is not recovered with the Ecosural, for which the heat release remains weaker for the dynamic model than for sigma all along the cycle. Therefore, it should not be considered that these two models have in general comparable behaviors. Despite these discrepancies between the SGS models in terms of flame surface, the associated in-cylinder pressure

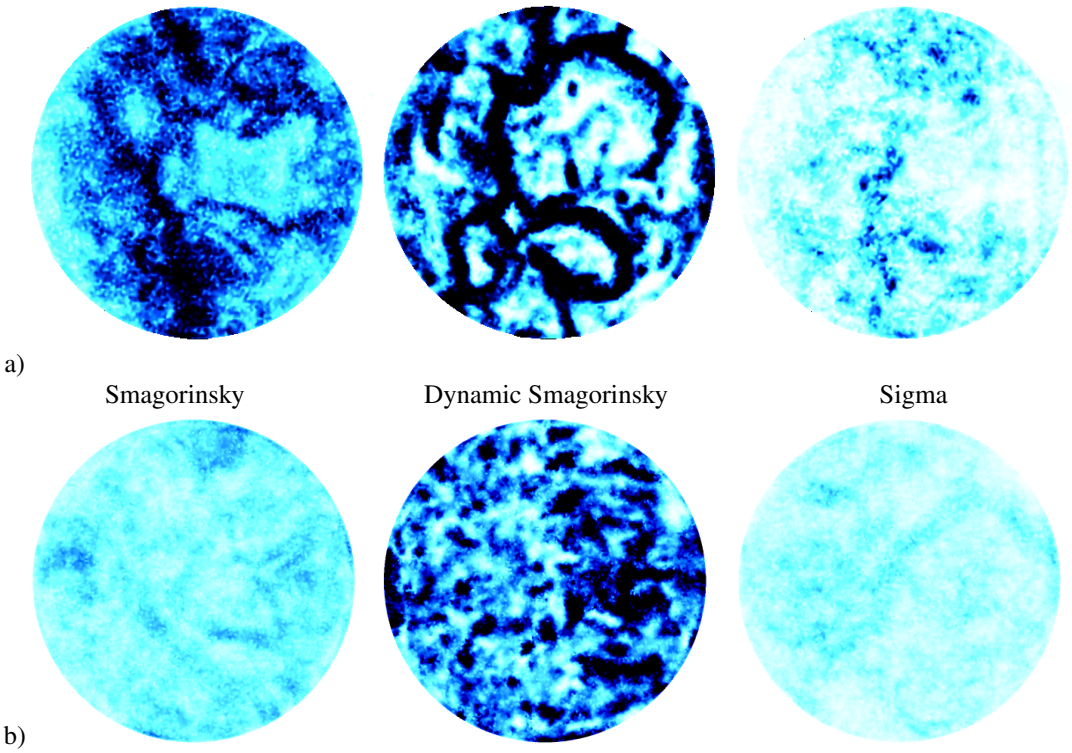

Figure 8
SGS viscosity fields at the piston for the three turbulence models : (a) F7P, (b) Ecosural.

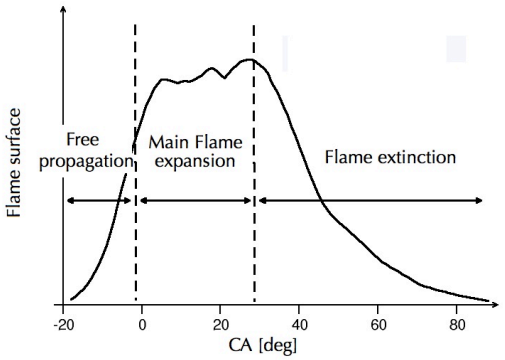

Figure 9
Flame propagation phases in ICE.

curves exhibit limited differences in the free propagation phase and globally stay within the Smagorinsky envelop of the F7P all along the cycle, as shown in Fig. 11. Only the sigma model leads to a slight overestimation of the pressure during flame kernel expansion, but its evolution is then close to the dynamic model one, which is coherent with previous findings on the heat release. Cylinder pressure curves from the Ecosural engines are not presented since no experimental data, and especially pressure envelopes, are available. This quantity thus does not bring additionnal information compared to flame surface evolutions.

To conclude this section, it can be stated that SGS models don't have a huge impact on global quantities such as the flow kinetic energy during intake and compression or the global heat release in the free flame propagation period. Sigma allows a little better resolution of flame-turbulence interactions and could be preferred to the classical Smagorinsky model. On the contrary the dynamic model shows non-physical behaviors at the walls at the end of compression and during combustion . It may thus be avoided to guaranty that flame propagation is not perturbed by this phenomenon in the two last phases of the heat release process.

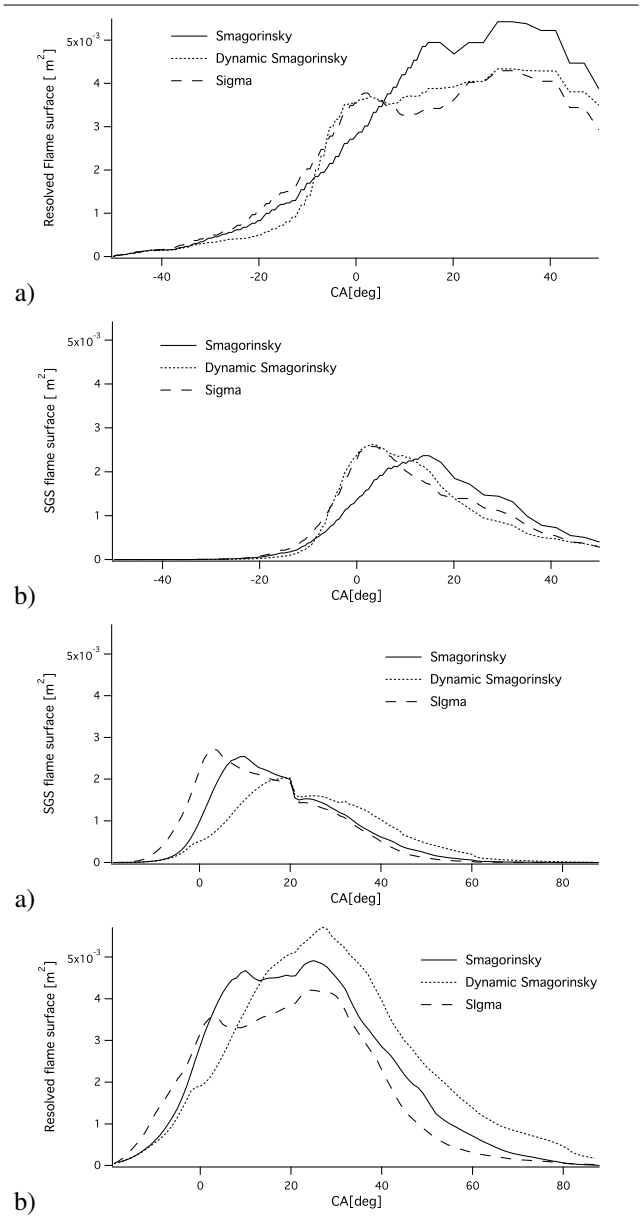

Figure 10
Resolved (a) and SGS (b) flame surface for Smagorinsky, Dynamic Smagorinsky and sigma models : top - F7P, bottom - Ecosural.

3.4 Restitution times

In terms of numerical costs, the SGS turbulence models used have no major impact as reported in Table 6. Only a small increase of the order of 5% is found for dynamic Smagorinsky which was expected because of the extra calculation needed to compute the constant. The choice of the SGS model may thus be more guided by stability and physical behavior criteria than computational ressources considerations.

TABLE 6
Restitution time normalized by the Smagorinsky restitution time.

	F7P	Ecosural
Smagorinsky	1	1
Dynamic Smagorinsky	1.05	1.07
sigma	0.99	1.002

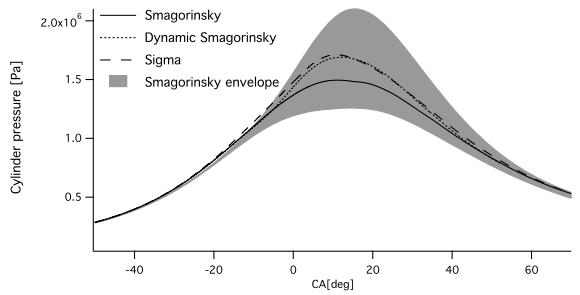

Figure 11

Mean in-cylinder pressure for Smagorinsky, Dynamic Smagorinsky and sigma models for F7P engine. Smagorinsky envelop is extracted from [16].

4 HIGH ORDER NUMERICAL SCHEMES IMPACT ON LES OF ICE

In this section, the different numerical schemes (LW, TTGC and TTG4A) are evaluated on the *unst_dil* operating point of the F7P engine and on the *knock* operating point of the Ecosural configuration. In all computations, the SGS model is the constant coefficient Smagorinsky ($Cs = 0.18$) and all parameters of the models are the same. For the F7P engine, in practice, only the TTGC and TTG4A simulations have been performed since LW simulations were already performed in [16]. Restitution time are presented in Table 7. Contrary to SGS models, CPU costs are very sensitive to the numerical scheme used. As expected, the order increase of TTG schemes comes with additional simulation costs by a factor close to 2. In the following, as for the SGS models, comparisons between the different schemes are based on the trapped mass, intake and compression flow motion and finally on the combustion process.

TABLE 7

Restitution time normalized by the LW one

F7P engine		
	LW	1
	TTG4A	1.91
	TTGC	1.84
Ecosural engine		
	LW	1
	TTG4A	1.84
	TTGC	1.82

4.1 LW - TTGC - TTG4A comparison for LES of ICE

4.1.1 Trapped mass

Table 8 summarizes the computed trapped mass for the three numerical schemes. The differences are slightly higher than for the SGS models but remain very limited ($\approx$ 1%). This quantity is thus almost insensitive to any variations in the numerical set-up.

TABLE 8

Computed trapped mass [mg] for the three numerical schemes.

	LW	TTG4A	TTGC
F7P	254	251.5	251.1
Ecosural	842.0	843.0	842.7

4.1.2 Intake and compression aerodynamics

Figure 12 shows instantaneous x-velocity profiles along the cylinder axis obtained with LW, TTGC and TTG4A at four distinct crank angles as well as the LW envelope extracted from [16] for the F7P engine.

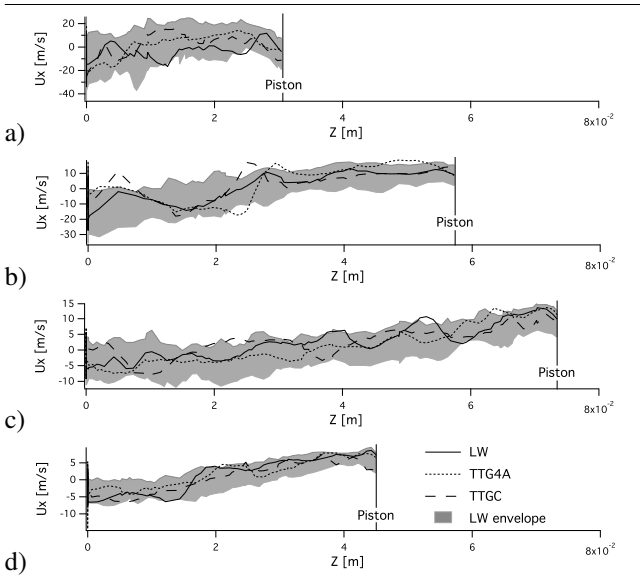

Figure 12

x-velocity profiles along the cylinder axis for the LW, TTGC and TTG4A schemes at -280 CAD (a), -240 CAD (b), -180 CAD (c) and -100 CAD (d). The LW envelope is extracted from [16]. The abscissa $z = 0$ corresponds to the bottom of the cylinder head.

Whatever the crank angle, all TTG profiles differ from the LW ones but remain very similar and lie within the statistical envelope. This observation holds true for the two other velocity components (not shown). As well, kinetic energy evolutions are similar for all schemes as shown in Fig. 13. In particular, the same rapid resolved energy drop at the end of the intake stroke and during compression is retrieved. It is particularly interesting to notice that the same observation can be made for both F7P and Ecosural configurations even if the flow energy levels differ a lot during intake.
At this point, it is of course impossible to claim that a numerical scheme is better than another: no pathologic behavior is noticed whatever the numerical scheme and all the results

remain within the range of cycle-to-cycle variations. However, little differences can be identified if a closer look is made on velocity fields (Fig. 14 and 15). Here again, the overall flow motion and the biggest structures resolution is similar for all schemes. Nevertheless, one should notice that the higher order feature of TTG schemes as a direct impact on convection of the smallest structures. Where LW tends to smooth these small gradients, TTG and especially TTGC is able of a better accuracy because of less dissipation and diffusion. This behavior can be retrieved on turbulent viscosity levels shown in Fig. 16. During the intake and compression phases, a sensibly higher level of turbulent viscosity is identifiable for TTG schemes and mostly for TTGC even if the Smagorinsky SGS model is used in all cases with the same constant $C_s = 0.18$. Differences can then only come from variations in the Reynolds tensor used by the model i.e. in the flow resolution. It results that a higher turbulent viscosity can be linked to more velocity gradients and in this case to less dissipation/diffusion of the smallest scales.

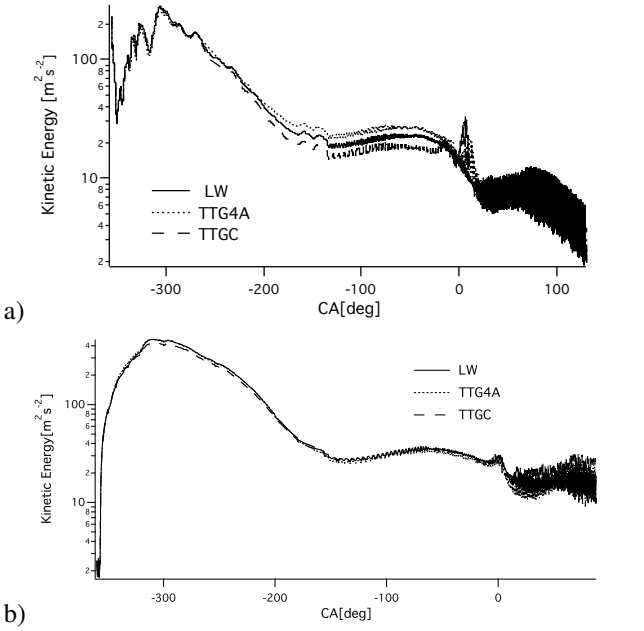

Figure 13
Kinetic energy evolution for F7P (a) and Ecosural (b) engines.

4.1.3 Combustion process

Regarding the combustion stroke, as for SGS models, single cycle computations only allow a comparison of the free expansion phase since in the second part of the flame propagation process, statistical results are compulsory to draw reliable conclusions. In all cases, a good resolution of the combustion is obtained given that the SGS flame surface never exceeds 30% of the total flame surface as shown in Fig. 17 and 18.
During this free expansion phase, that is to say almost until TDC for both engines, more flame surface is obtained with TTG schemes. To be more specific, the difference mainly appears at the resolved level (Fig. 17 and 18). Although the resolved flow fields don't exhibit huge differences in terms of kinetic energy and flow structures, TTG schemes leads to more resolved flame surface. This higher flame surface implies a higher heat release rate and then a faster combustion as confirmed by in-cylinder pressures which are out of CCV envelopes for the F7P engine (Fig. 19(a)), and this even in the very beginning of combustion.
Although, the better resolution of flame wrinkling in TTG cases can explain a faster combustion, it can not only be due to the flow resolution at spark timing. Indeed, the presence of high strain zones in the LW flow field at ignition, as shown in Fig. 14 (c) and 15 (c), should balance the dissipation and the diffusion which prevent a proper convection of the smallest structures. It is therefore likely that the resolved flame surface increase is due to a less dissipation and diffusion in the reaction zone with TTG schemes, allowing a better resolution of flame-turbulence interactions.

To summarize, a slight improvement is obtained for the flow field resolution especially with TTGC. In addition, the higher order feature of TTG schemes permits a better resolution of the combustion phase and in particular of the flame wrinkling process. The resolved flame surface is therefore higher with high order schemes. However, since all the schemes should simulate the same flame (during the free expansion flame at least), the same amount of total flame surface should be retrieved and an increase in the resolved contribution should lead to lower SGS flame surface which is not the case here. Non-realistic flame development is then found with TTG schemes and in-cylinder pressure are out of the CCV envelope from Granet *et al.* [16].

4.2 The efficiency model

The higher order of TTG schemes is supposed to provide high fidelity and reliability in the description of the flow and combustion compared to LW. However the results of section 4.1.3 show that non realistic levels of pressure are reached when those schemes are used. To understand this non expected behavior, a deeper analysis of the combustion process and its modeling are required. In this study, combustion is modeled with the Thickened Flame LES model (TFLES) [6]. In this approach, the flame is artificially thickened in order to ensure an appropriate resolution of the flame front on the LES grid. But when the flame is thickened, the combustion-turbulence interaction is affected, reducing flame wrinkling at the resolved level and obliging to model the lost part at the SGS level. This role is fulfilled by the efficiency function E, which is given by Eq. 36 in the paper of Colin *et al.* [6]:

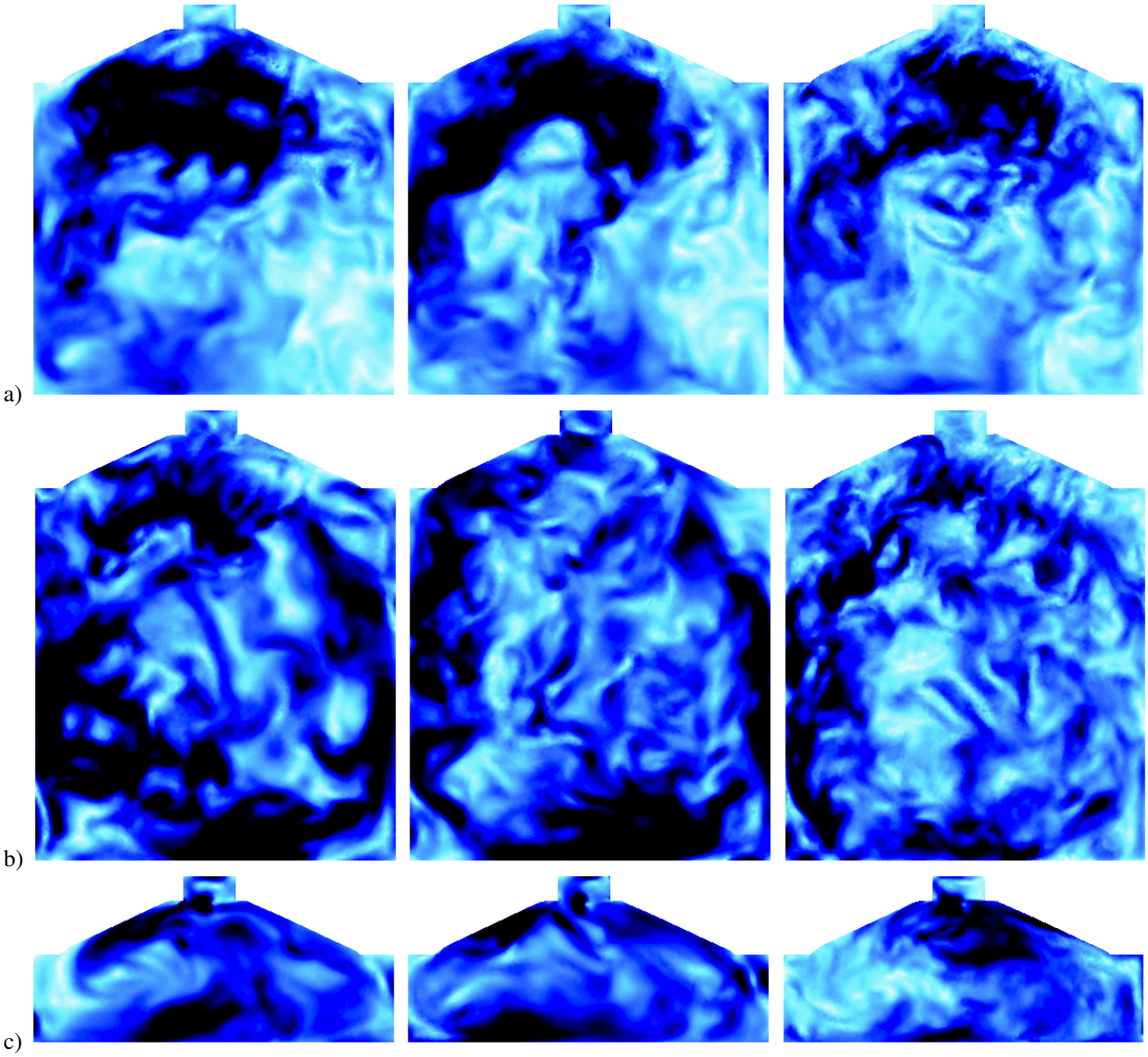

Figure 14

Velocity fields at the cylinder center (Y=0) for the LW, TTG4A and TTGC schemes at -240 CAD (a), -180 CAD (b) and -50 CAD (c) for the F7P engine.

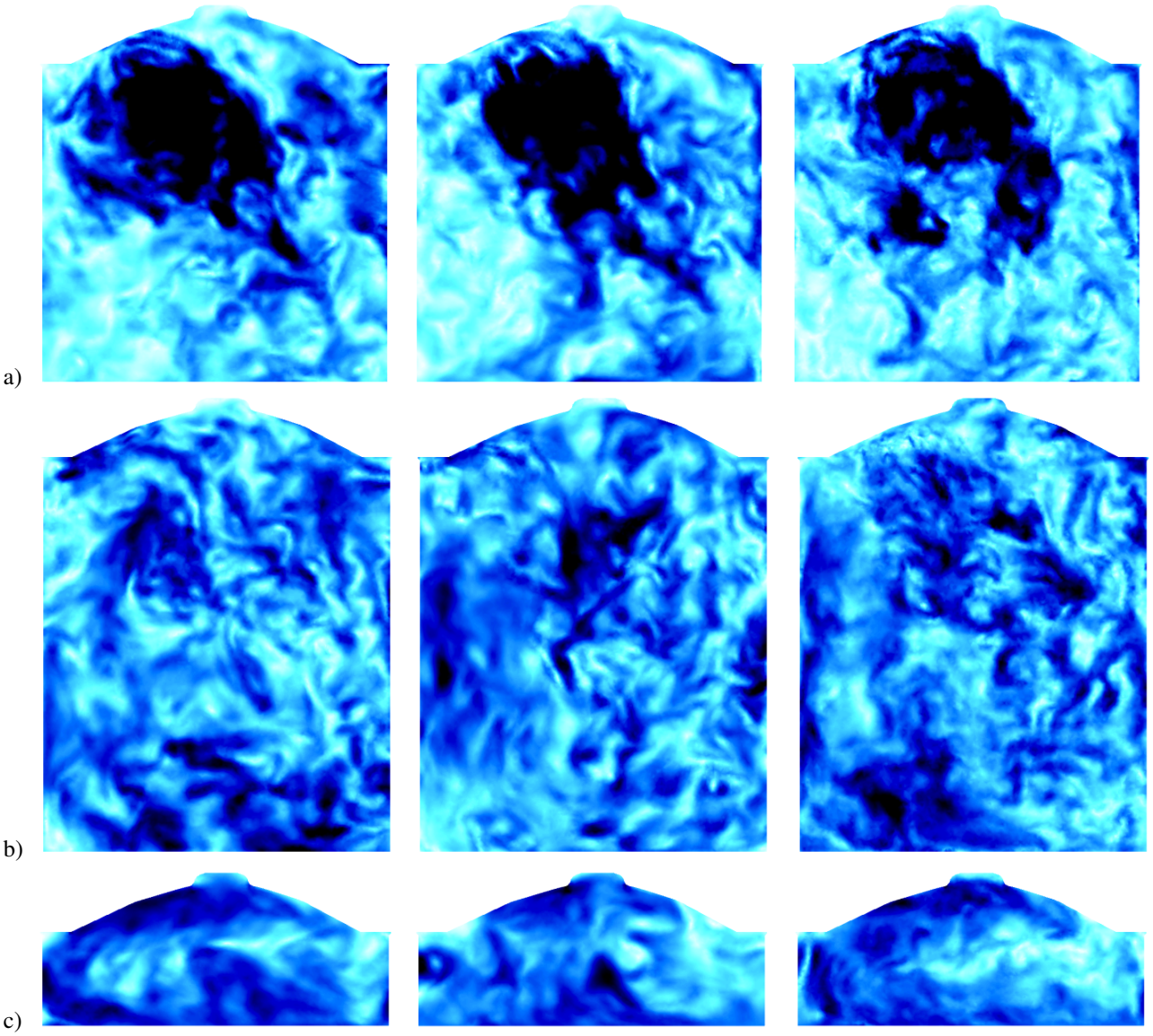

Figure 15

Velocity fields at the cylinder center (Y=0) for the LW, TTG4A and TTGC schemes at -240 CAD (a), -180 CAD (b) and -50 CAD (c) for the Ecosural engine.

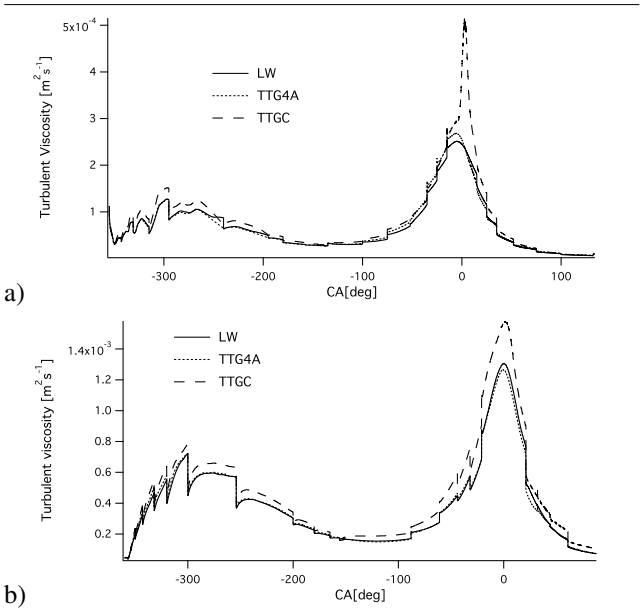

Figure 16

Turbulent viscosity evolution for the F7P (a) and the Ecosural (b) engines.

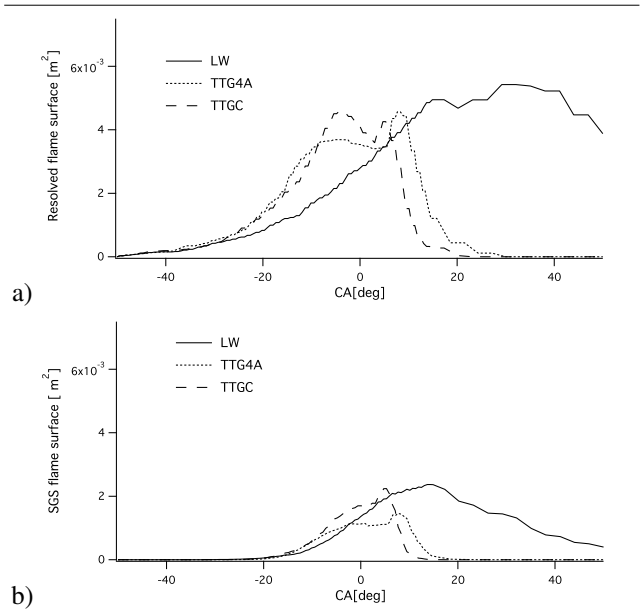

Figure 17

Resolved (a) and SGS (b) flame surfaces for the F7P engine.

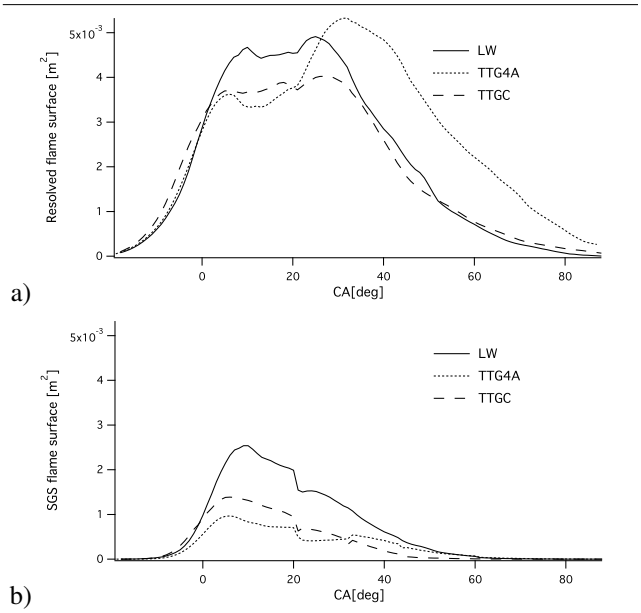

Figure 18

Resolved (a) and SGS (b) flame surfaces for the Ecosural engine.

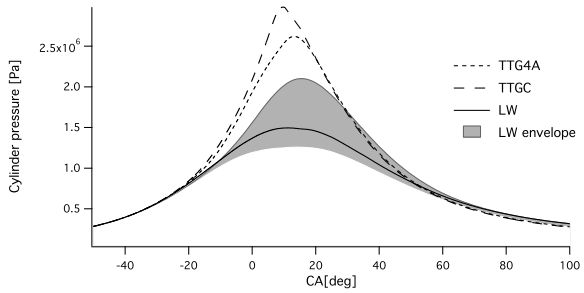

Figure 19

In-cylinder pressure for F7P engine. The LW envelope is extracted from[16].

$$E = \frac{\Xi(\delta_l^0)}{\Xi(\delta_l^1)} \tag{1}$$

where $\Xi(\delta_l^1)$ and $\Xi(\delta_l^0)$ are respectively wrinkling factors corresponding to thickened and non thickened flames estimated by:

$$\Xi(\delta) = 1 + \alpha\Gamma\left(\frac{\Delta_e}{\delta}, \frac{u'}{s_l^0}\right)\frac{u'}{s_l^0} \tag{2}$$

with Γ a function of the SGS strain rate, u' the fluctuating velocity, Δ_e the filter size , s_l^0 the laminar flame speed and α a constant given by:

$$\alpha = \beta\frac{2ln(2)}{3c_{ms}\left[Re^{1/2} - 1\right]} \tag{3}$$

In this expression, β is the TFLES model constant and c_{ms} another constant fixed to 0.28 using the DNS results by Yeung *et al.* [34]. The only parameter which changes, depending on the numerical scheme used, is the fluctuating velocity since the meshes and operating conditions are kept constant. An estimation of this velocity based on the resolved velocity field laplacian is given by [6]:

$$u' = 2\Delta_x^3 rot(\nabla^2\bar{\mathbf{U}}) \tag{4}$$

with $\bar{\mathbf{U}}$ the resolved velocity vector. When using the TFLES model, users have to fix the β constant which is recommended to be of the order of unity by Colin *et al.* [6]. In this work, it is set to 2, in accordance with previous engine simulations. Indeed, this value was used in several former computations on different engine configurations, in particular the F7P engine considered in this work and the XU10 engine described in [28, 32]. It has to be noted that these multi-cycle LES were all performed with the LW scheme. However, in order to ensure a fair comparison between the different numerical schemes, the value $\beta = 2$ was kept for all the simulations, even for TTGC and TTG4A.

The SGS velocity is clearly higher in the two TTG simulations and especially with TTGC during the whole combustion process. Since the constant β is identical for the three schemes, this higher intensity in the SGS velocity will then generate higher values of E and finally higher SGS flame surface and heat releases. Given the fact that i) both TTGC and TTG4A schemes "should" resolve a larger part of the heat release compared to LW; ii) TTG schemes are classically used in other fields of application with an efficiency constant $\beta = 0.3$ [33]; new computations have been performed with this new value $\beta = 0.3$. Figure 20 shows the impact of this new constant on the in-cylinder pressure for the TTGC case: the pressure decreases as expected and almost gets back within the reference envelope.

This test reveals that a constant $\beta = 2$ leads to an overestimation of the efficiency function in the case of a TTG

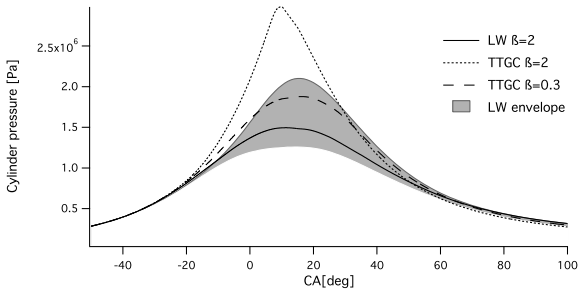

Figure 20

Impact of the efficiency constant β of the efficiency combustion model on the in-cylinder pressure for the F7P engine. LW envelop is extracted from [16].

scheme and forces a too rapid propagation of the flame. Table 9 presents the classical indicators CA2, CA10, CA50 and CA90, where CAX is defined as the timing for which the burnt mass fraction reaches $X\%$.

TABLE 9

Main characteristic times of the combustion process. CA are given with reference to the ignition time[16].

	ca2	ca50	ca90
Exp. enveloppe	[37-48]	[58-84]	[77-132]
LW, $\beta = 2$	44	77.5	92
TTGC, $\beta = 2$	34	41	60
TTGC, $\beta = 0.3$	38	66	87

As reported in [16], an efficiency constant $\beta = 2$ associated to LW provides good estimations of the different combustion times compared to experimental observations. With TTGC and $\beta = 2$, the combustion is far too fast and none of the CAX are in the experimental envelope. For $\beta = 0.3$ and TTGC, combustion times get back in this envelope.

These results are consistent with Fig. 21 which shows the resolved and SGS flame surfaces for the three cases of Table 9. Still during the free propagation phase, both the resolved and SGS parts are larger with TTGC/$\beta = 2$ than with LW. The resulting total flame surface and thus heat release is larger for TTGC and leads to an overestimation of the cylinder pressure. For $\beta = 0.3$ and TTGC, the resolved contribution is still larger than for LW and $\beta = 2$ but the SGS contribution is lower. In this case, the two contributions nearly balance and the total heat release reaches similar values than LW.

Although is it obviously delicate to draw definitive conclusions with only single-cycle computations, the different tests suggest that using the same constant in the efficiency function whatever the numerical scheme may lead to highly erroneous results. This is not so surprising. Efficiency functions and their constant are classically built using Direct Numerical Simulations of flame-vortex or flame-HIT interactions [4, 6] using high order numerical schemes (typically

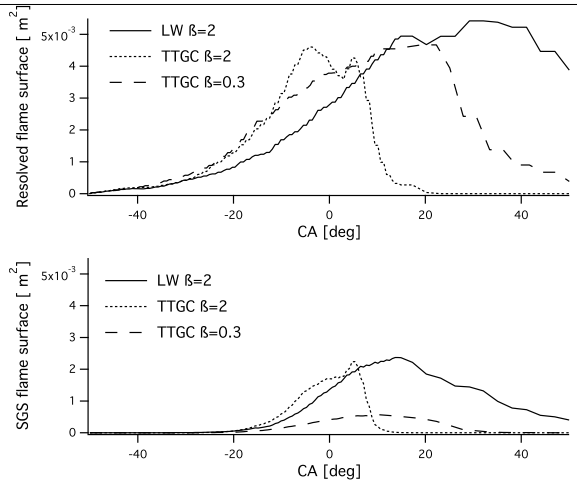

Figure 21

Impact of the efficiency constant on flame surface contributions for F7P engines.

sixth-order compact schemes). The response of the flame to the turbulence is then studied for various thickening factors varying the mesh size Δ_x. In that sense, the results are directly related to the spatial order of the numerical scheme used and to its intrinsic properties (dispersion and dissipation). It is thus highly probable that, if the same kind of test would be performed with LW and TTGC schemes, different values of the efficiency constant would be found. In that way, changing this constant depending on the numerical scheme used makes sense.

For the present computations, the value $\beta = 2$ used in LW computations is necessary to obtain reasonable results because it certainly allows to compensate the SGS part of the resolve contribution that has been dissipated by the numerical scheme. For a numerical scheme with better dissipative properties like TTGC or TTG4A, this overestimation of the efficiency constant is not needed anymore. For the presented simulations, the two combinations TTGC/$\beta = 0.3$ and LW/$\beta = 2$ give very similar results. However, this result is due to different mechanisms: for LW/$\beta = 2$, a large part of the combustion is due to SGS phenomena (up to 35% of the total heat release) whereas for TTGC/$\beta = 0.3$ combustion is dominated by resolved phenomena since the SGS contribution never exceeds 12% of the total heat release. Obviously this last situation is highly preferable since it allows to reduce the influence of empirical inputs on the final result. This does not mean that the LW/$\beta = 2$ computation is wrong but one can suppose that this set up will be more likely to be invalid for other engine geometries or operating points for instance.

5 EVALUATION OF A NEW HYBRID APPROACH

Following the results of section 3, the influence of SGS models on LES findings may mainly be considered as a numerical perturbation. The constant coefficient Smagorinsky model, which is the classical SGS closure used for engine piston computations, is thus preferred to the dynamic procedure or sigma in this section.

Numerical schemes were evaluated in section 4 and presented a limited influence on the flow evolution during intake and compression, even if TTG schemes allowed a slightly better resolution of the velocity field. This may be explained by the well-refined LES grids used in this study allowing to directly capture the main part of the flow energy on the mesh. This is also because large structures are found during intake and compression, and the tumble motion breakdown process, which produces small scale turbulence, mainly occurs at the end of compression and in the first instant of combustion. On the contrary, huge discrepancies were observed during combustion, where higher order schemes permitted a higher resolution of the flame wrinkling on the grid, due to an improved description of flame-turbulence interactions. Nevertheless, the drawback of high order schemes is that more calculation resources are needed, and it is one of the main reason explaining the extensive use of LW in previous engine LES studies.

Starting from these conclusions, a natural idea is to split the engine cycle in two separate parts, namely intake-compression and combustion, and to use dedicated numerical set-up for each one to optimize both precision and CPU cost. Therefore, TTGC may be used during combustion, while LW may be retained for the rest of the cycle (intake, compression, end of expansion and exhaust).

However it is important to keep in mind that this hybrid approach is limited to homogeneous cases. In very heterogeneous configurations like direct injection of fuel or controlled auto-ignition, TTGC could be activated during engine compression to keep a good resolution of temperature and mixture stratifications, phenomena which are of first order in such cases.

The proposed hybrid approach is called ESO_2 (Engine Stroke Optimal Order), and is analyzed in the following using once again the two engine configurations presented in section 2.2. For each engine, all simulations are performed keeping the same $\beta = 0.3$ constant in the efficiency function of the TFLES model in order to perform fair comparisons from the numerical point of view.

5.1 Flow motion during combustion

For an ESO_2 calculation, TTGC is imposed only 2 CAD before ignition. This period prior to ignition corresponds to a too short time interval for affecting the initial LW velocity field, and ESO_2 results don't present significant changes

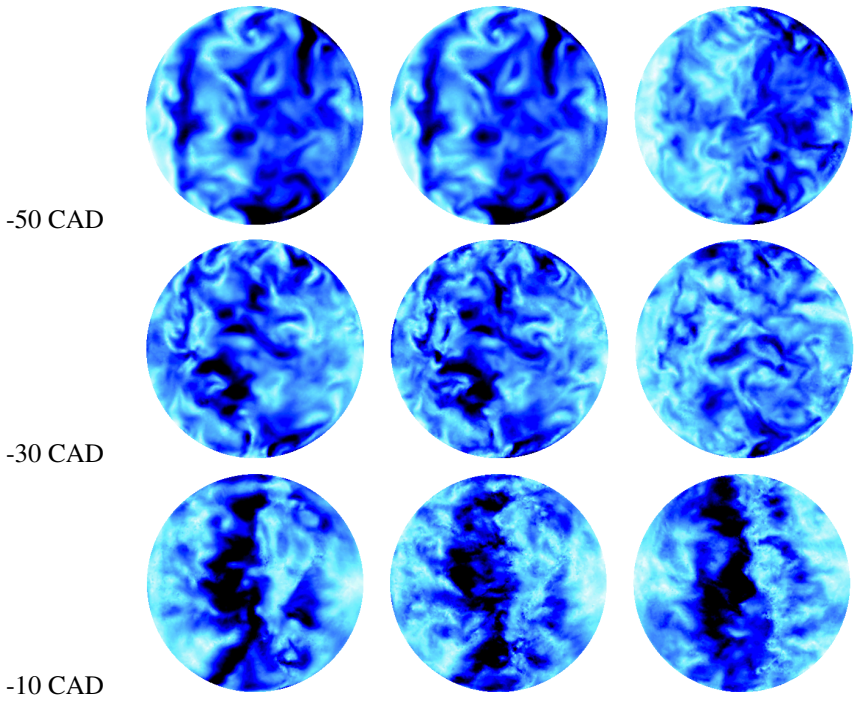

Figure 22
Velocity fields at different CA for LW (left), $ES\,O_2$ (middle) and TTGC (right) for the F7P engine.

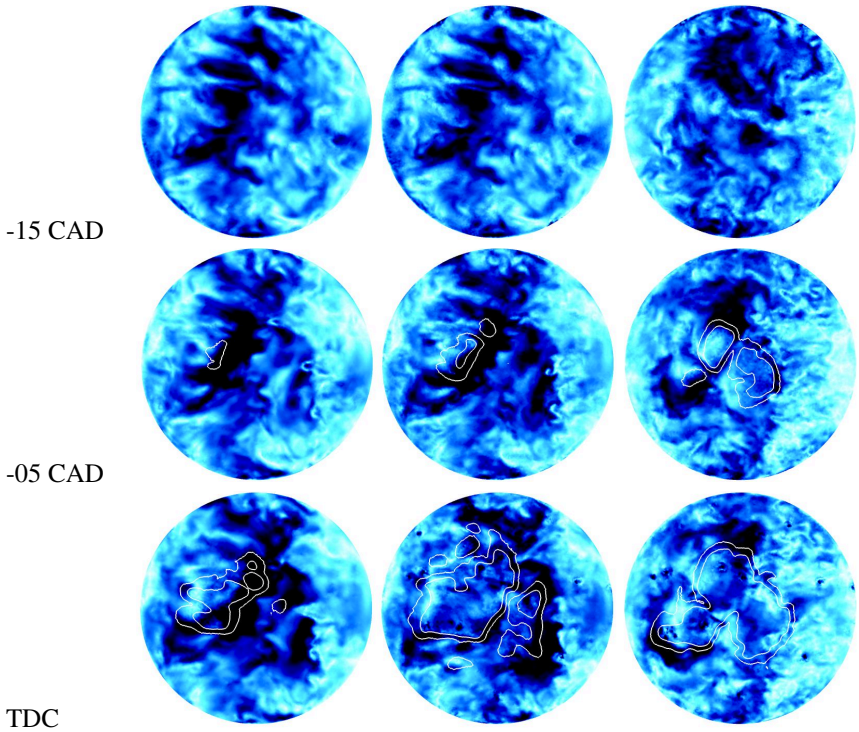

Figure 23
Velocity fields at different CA for LW (left), $ES\,O_2$ (middle) and TTGC (right) for the Ecosural engine.

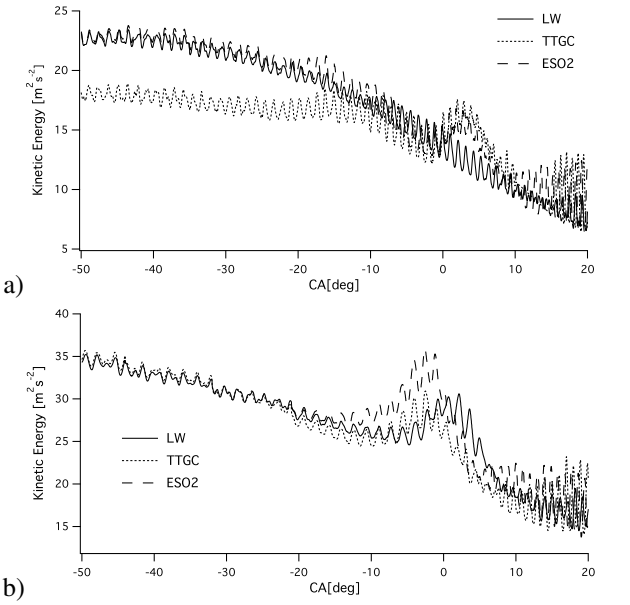

Figure 24

Resolved kinetic energy evolution during the engine cycle for LW, ESO2 and TTGC : F7P (a) and Ecosural (b).

with respect to LW as displayed in Fig. 22 and 23. Engine flow motion differences are thus only analyzed during the combustion phase in this section. During the whole free propagation phase, a memory effect is visible on the velocity field of the ESO_2 computation as shown in Fig. 22 and 23. Indeed, the ESO_2 field looks like the LW one, while the burnt mass fraction is lower than 10%, and the TTGC simulation still presents more turbulent structures than the two other cases. Then, combustion has an important effect on the flow, because of the fast thermal expansion of burnt gases, and higher differences are obtained between LW and ESO_2. When the burnt mass fraction reaches 50%, the ESO_2 velocity field even presents small eddies and is more comparable to the TTGC one. This statement remains true for both engines and is confirmed by Fig. 22 and 23, which shows a slightly lower dissipation during combustion with the hybrid method than for LW and ESO_2 levels gradually joins those of the full TTGC run.

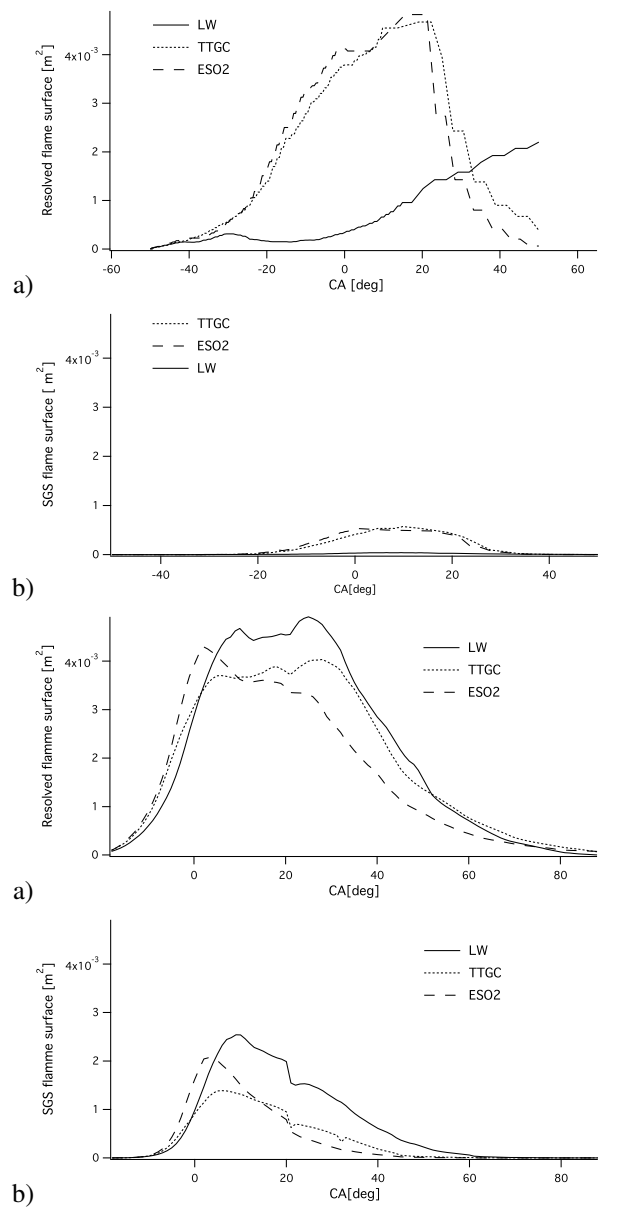

Figure 25

Resolved (a) and SGS (b) flame surface for LW, ESO_2 and TTGC : F7P (a) and Ecosural (b).

5.2 Flame propagation process

Evolutions of the resolved and SGS flame surfaces are plotted in Fig. 25 for the two engine configurations. An important feature of the F7P engine is that the LW combustion is too slow with an efficiency model constant of 0.3 (Fig. 21). The resulting flame surface is then quite low compared to others numerical schemes, especially at the resolved level.
During the free propagation of the flame, the resolved surface associated to ESO_2 is higher than the LW one and is more comparable to a full TTGC simulation. However, as described previously, the LW and ESO_2 cases have flow fields which differ from the TTGC one, especially close to the spark plug. Flame-turbulence intqeractions are thus deeply affected, and comparisons between ESO_2 and TTGC can not be directly performed. The ESO_2 cycle may indeed be considered as a numerical perturbation of a full TTGC engine cycle during the first part of the cycle (intake and compression).
At the SGS level, TTGC and ESO_2 also give higher surfaces than LW. This is notably due to their higher resolved flame

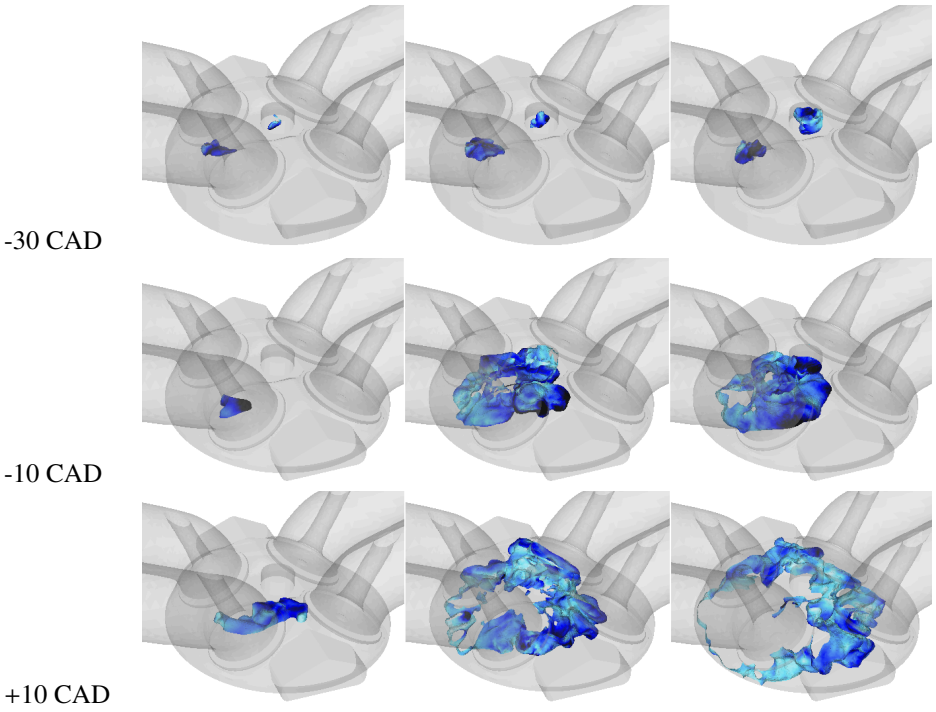

Figure 26
Progress variable iso-surface at different CA for the F7P engine.

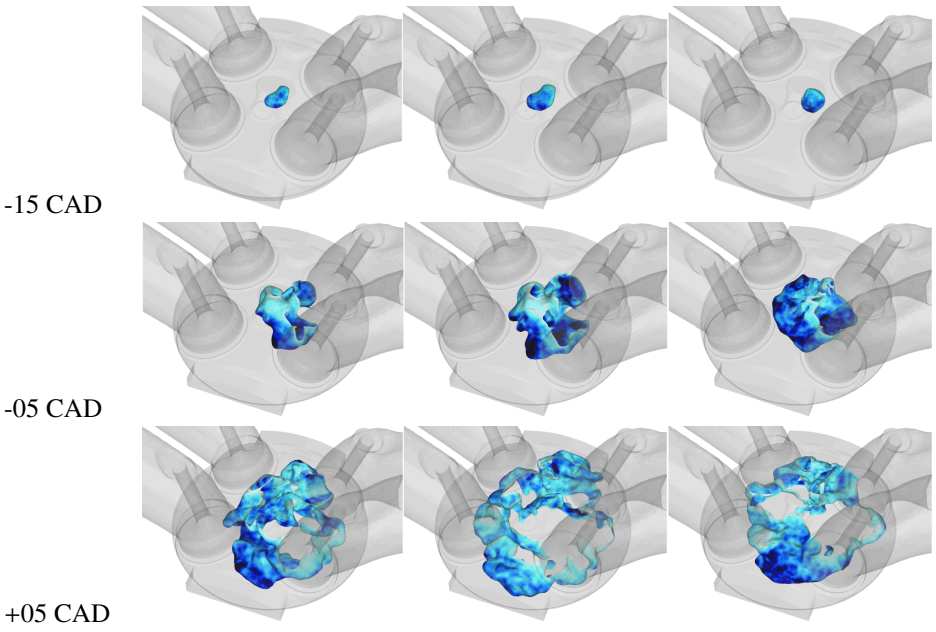

Figure 27
Progress variable iso-surface at different CA for the Ecosural engine.

surface. Nevertheless, whatever the scheme used, the SGS surface stays lower than the resolved surface, confirming the good quality of the computational grid used in the two configurations.

The analysis of progress variable iso-surfaces based on fuel concentrations, plotted at different crank angles in Fig. 26 and 27, reinforces previous conclusions. The ESO_2 flame shape remains close to the LW case and underlines the impact of the velocity field history effect at spark timing on flame-turbulence interactions. However, the propagation is faster for ESO_2 than for LW, and the flame expansion velocity is close to the TTGC case, then leading to similar cylinder pressure curve evolutions as shown in Fig. 28. This observation corroborates the idea that the ESO_2 calculation can be view as a perturbed TTGC engine cycle.

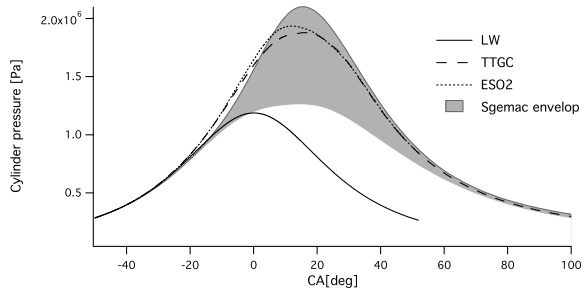

Figure 28

Mean in-cylinder pressure for TTGC, LW and ESO_2.

5.3 CPU time

All the achieved simulations include intake, compression and combustion phases. In other words, no more than about half a cycle is simulated (from -355 CAD to 50 CAD for F7P configuration, and from -360 CAD to 88 CAD for Ecosural configuration). In order to evaluate the potential CPU costs improvements associated to ESO_2, an extrapolation is performed over a whole cycle assuming a TTGC-LW switch when the combustion ends, i.e. at 50 CAD (resp. 90) for the F7P (resp. for Ecosural) configuration. The estimated restitution times are given in Table 10.

The CPU over cost of TTGC is reduced of about 84% using the ESO_2 method, due to the low combustion duration. Thus, the obtained CPU time remains in line with previous engine LES simulations, while an increase precision can be expected. The proposed hybrid approach finally appears promising for LES studies of industrial configurations.

TABLE 10

Estimated restitution time normalized by the LW restitution time. The constant coefficient Smagorinsky is used for all cases.

	F7P	Ecosural
LW	1	1
ESO_2	1.08	1.15
TTGC	1.84	1.82

6 CONCLUSION

The objective of this study was therefore to evaluate the feasability and possible benefits of using high order schemes and state of the art sgs models in LES of ICE. For this purpose a first part was dedicated to the comparison of several SGS turbulence models, namely the constant coefficient and dynamic Smagorinsky and the sigma closure, keeping the Lax Wendroff scheme for all simulations. It was shown that the sigma model allows a slightly better resolution of the velocity field because of a lower SGS vicosity and a few improvements in the resolution of flame-turbulence interactions, without additionnal CPU time. On the contrary the dynamic model generates high viscosity level, especially at the walls, which is not a physical behavior, with a small increase (about 5%) of computational times. Nevertheless, discrepancies between the models were low and all quantities remained in the CCV envelopes, suggesting that the change in SGS closure mainly acts like a numerical perturbation of the flow. In a second part, two convective schemes from the Taylor-galerkin family, namely TTGC and TTG4A were compared to the classical Lax Wendroff one. Numerical findings indicate that all set-up lead to similar evolutions of the flow properties (kinetic energy, SGS viscosity) during compression and intake even if a little more turbulent structures were found for TTG schemes, maybe due to the quality and high resolution of the LES grid used for both cases. However, the free flame propagation exhibited completely different behaviors between the schemes. TTG4A, and even more TTGC, were characterized by increased resolved flame surface levels, probably due to lower diffusion fluxes in the reaction zone then allowing a better resolution a flame-turbulence interactions. This phenomenon led to very different in-cylinder pressures, which were not included in CCV envelopes anymore. A further analysis of the SGS combustion model allowed to demonstrate that the efficiency function constant should be reduced when using TTG models because a larger part of the flame wrinkling is directly resolved on the grid. However, restitution times were doubled with the higher order schemes. All these results brought the idea of combining LW during intake and compression, where differences with TTGC are low, and TTGC during combustion to better resolve the flame. This approach, called ESO_2 (Engine Stroke Optimal Order), showed results very close to TTGC, with reasonnable additionnal CPU cost (about 10%) compared to LW. The fact that for the whole study same findings were obtained for both engine configurations, operating in very different conditions, may confer them a general character, even if statistics should be necessary to draw definitive conclusions. Finally, ESO_2 appears

as a promising method for future LES studies of ICE. This approach may be ideally used with the sigma model. However, first tests indicate that combining sigma with TTGC may lead to numerical instabilities because of the very low levels of viscosity in the calculation. As the constant coefficient Smagorinsky model gave results quite close to those of sigma, it could also be retained for future practical applications in complex geometries.

7 ACKNOWLEDGMENTS

This work was granted access to the HPC resources of CCRT under allocations 2012-026139 and 2012-026074 made by GENCI (Grand Equipement National de Calcul Intensif).

REFERENCES

1 URL http://www.agence-nationale-recherche.fr/projet-anr/?tx_lwmsuivibilan_pi2%5BCODE%5D=ANR-10-VPTT-0002.

2 I. Celik, I. Yavuz, A. Smirnov, J. Smith, E. Amin, and A. Gel. Prediction of in-cylinder turbulence for IC engines. *Combustion Science and Technology*, 153:339–368, 2000.

3 I. Celik, I. Yavuz, and A. Smirnov. Large eddy simulations of in-cylinder turbulence for internal combustion engines: a review. *Int. J. Engine Research*, 2(2):119–148, 2001.

4 F. Charlette, D. Veynante, and C. Meneveau. A power-law wrinkling model for LES of premixed turbulent combustion: Part I - non-dynamic formulation and initial tests. *Combustion and Flame*, 131:159–180, 2002.

5 O. Colin and M. Rudgyard. Development of high-order Taylor-Galerkin schemes for unsteady calculations. *Journal of Computational Physics* , 162(2):338–371, 2000.

6 O. Colin, F. Ducros, D. Veynante, and T. Poinsot. A thickened flame model for large eddy simulations of turbulent premixed combustion. *Phys. Fluids* , 12(7):1843–1863, 2000.

7 V. Dugue, N. Gauchet, and D. Veynante. Applicability of large eddy simulation to the fluid mechanics in a real engine configuration by means of an industrial code. *SAE paper*, (2006-01-1194), 2006.

8 B. Enaux, V. Granet, O. Vermorel, C. Lacour, C. Pera, C. Angelberger, and T. Poinsot. LES and experimental study of cycle-to-cycle variations in a spark ignition engine. *Proc. Combust. Inst.*, 33:3115–3122, 2011.

9 B. Enaux, V. Granet, O. Vermorel, C. Lacour, L. Thobois, V. Dugué, and T. Poinsot. Large eddy simulation of a motored single-cylinder piston engine: Numerical strategies and validation. *Flow, Turbulence and Combustion*, 86(2):153–177, 2011.

10 B. Fiorina, R. Vicquelin, P. Auzillon, N. Darabiha, O. Gicquel, and D. Veynante. A filtered tabulated chemistry model for les of premixed combustion. *Combustion and Flame*, 157(3):465–475, 3 2010.

11 J-B. Michel G. Lecocq, S. Richard and L. Vervisch. A new les model coupling flame surface density and tabulated kinetics approaches to investigate knock and pre-ignition in piston engines. *Proc. Combust. Inst.*, 33(6):1215–1226, 20111.

12 M. Germano, U. Piomelli, P. Moin, and W. Cabot. A dynamic subgrid-scale eddy viscosity model. *Phys. Fluids* , 3(7):1760–1765, 1991.

13 D. Goryntsev, A. Sadiki, M. Klein, and J. Janicka. Large eddy simulation based analysis of the effects of cycle-to-cycle variations on air-fuel mixing in realistic DISI IC-engines. *Proc. Combust. Inst.*, 32:2759–2766, 2009.

14 N. Gourdain, L. Gicquel, M. Montagnac, O. Vermorel, M. Gazaix, G. Staffelbach, M. Garcia, J.F. Boussuge, and T. Poinsot. High performance parallel computing of flows in complex geometries: I. methods. *Comput. Sci. Disc.*, 2: 015003, 2009.

15 N. Gourdain, L. Gicquel, G. Staffelbach, O. Vermorel, F. Duchaine, J-F. Boussuge, and T. Poinsot. High performance parallel computing of flows in complex geometries - part 2: applications. *Comput. Sci. Disc.*, 2(1):28pp, January-December 2009.

16 V. Granet, O. Vermorel, C. Lacour, B. Enaux, V. Dugué, and T. Poinsot. Large-eddy simulation and experimental study of cycle-to-cycle variations of stable and unstable operating points in a spark ignition engine. *Combustion and Flame*, 159: 1562–1575, 2012.

17 D. Haworth. Large-eddy simulation of in-cylinder flows. *Oil and Gas Science Tech.- Rev de l'IFP*, 54(2):175–185, 1999.

18 R. Jhavar and C. J. Rutland. Using large-eddy simulations to study mixing effects in early injection diesel engine combustion. *SAE paper*, (2006-01-0871), 2006.

19 G. Lacaze, E. Richardson, and T. J. Poinsot. Large eddy simulation of spark ignition in a turbulent methane jet. *Combustion and Flame*, 156(6):1993–2009, 2009.

20 C. Lacour and C. Pera. An experimental database dedicated to the study and modelling of cyclic variability in spark-ignition engines with les. *SAE paper*, (2011-01-1282), 2011.

21 C. Lacour, C. Pera, B. Enaux, O. Vermorel, C. Angelberger, and T. Poinsot. Exploring cyclic variability in a spark-ignition engine using experimental techniques, system simulation and large-eddy simulation. *Proc. of the 4th European Combustion Meeting*, 2009.

22 P. D. Lax and B. Wendroff. Difference schemes for hyperbolic equations with high order of accuracy. *Communications on Pure and Applied Mathematics* , 17:381–398, 1964.

23 C. Meneveau and T. Lund. The dynamic smagorinsky model and scale-dependent coefficients in the viscous range of turbulence. *Phys. Fluids* , 9(12):3932–3934, 1997.

24 Y. Morinishi, S. Tamano, and K. Nakabayashi. Direct numerical simulation of compressible turbulent channel flow between adiabatic and isothermal walls. *Journal of Fluid Mechanics*, 502:273–308, 2004.

25 C. Pera, S. Richard, and C. Angelberger. Exploitation of multi-cycle engine LES to introduce physical perturbations in 1D engine models for reproducing CCV. *SAE paper*, (2012-01-0127), 2012.

26 S. B. Pope. Ten questions concerning the large-eddy simulation of turbulent flows. *New Journal of Physics*, 6:35, 2004.

27 E. Riber, V. Moureau, M. García., T. Poinsot, and O. Simonin. Evaluation of numerical strategies for LES of two-phase reacting flows. *Journal of Computational Physics* , 228:539–564, 2009.

28 S. Richard, O. Colin, O. Vermorel, A. Benkenida, C. Angelberger, and D. Veynante. Towards large eddy simulation of

combustion in spark ignition engines. *Proc. Combust. Inst.*, 31:3059–3066, 2007.

29 M. Sanjosé, J. M. Senoner, F. Jaegle, B. Cuenot, S. Moreau, and T. Poinsot. Fuel injection model for euler–euler and euler–lagrange large-eddy simulations of an evaporating spray inside an aeronautical combustor. *International Journal of Multiphase Flow*, 37(5):514–529, 6 2011.

30 J. Smagorinsky. General circulation experiments with the primitive equations: 1. the basic experiment. *Mon. Weather Rev.* , 91:99–164, 1963.

31 H. Baya Toda, O. Cabrit, G. Balarac, S. Bose, J. Lee, H. Choi, and F. Nicoud. A subgrid-scale model based on singular values for LES in complex geometries. In *Proc. Summer Program*, volume 193. CTR, 2010.

32 O. Vermorel, S. Richard, O. Colin, C. Angelberger, A. Benkenida, and D. Veynante. Towards the understanding of cyclic variability in a spark ignited engine using multi-cycle LES. *Combustion and Flame*, 156(8):1525–1541, 2009.

33 P. Wolf, G. Staffelbach, A. Roux, L. Gicquel, T. Poinsot, and V. Moureau. Massively parallel LES of azimuthal thermo-acoustic instabilities in annular gas turbines. *Comptes Rendus Mécanique*, 337(6-7):385–394, 2009.

34 P. K. Yeung, S. S. Girimaji, and S. B. Pope. Straining and scalar dissipation on material surfaces in turbulence: implications for flamelets. *Combustion and Flame*, 79:340–365, 1990.

The date of receipt and acceptance will be inserted by the editor.